Magazine of Civil Engineering

ISSN 2712-8172

journal homepage: http://engstroy.spbstu.ru/

Research article

UDC 624

DOI: 10.34910/MCE.138.5



# Finite element analysis of fatigue damaged reinforced concrete one-way slabs repaired with CFRP sheets

***M.O. Hameed*** [1] ✉ , ***R.A. Daud*** [2]

[1] *College of Engineering, Al-Nahrain University, Baghdad, Iraq*

[2] *Al-Nahrain University, Baghdad, Iraq*

✉ *st.mohammed.a.h.f@nahrainuniv.edu.iq*

**Keywords:** ABAQUS, fatigue damage, EBR, CFRP sheet, one-way slab

**Abstract.** In twenty-eight samples in this study, the structural behavior of fatigue-damaged one-way slabs was produced using a nonlinear finite element model that was created using ABAQUS. The effect of carbon fiber-reinforced polymer (CFRP) parameters and fatigue-damaged percentages is examined to obtain a better reaction. The full model accounts for the elastic and plastic behavior of the materials and uses three-dimensional parts (solid, shell, and truss). To investigate the accuracy of the model, the authors' experimental data (monotonic and fatigue damage) is used to validate the numerical outputs. For the four verified slabs, the average and coefficient of variations for ultimate load of finite element analysis to ultimate load of experimental work were 0.997 and 5.35 %, respectively; for the deflection of finite element analysis to deflection of experimental work, they were 1.197 and 15.99 %, and for energy absorption, they were 1.134 and 12.2 %, respectively. Twenty-four samples parametric studies using the impacts of CFRP sheet thickness, CFRP sheet modulus of elasticity, CFRP sheet length, the concrete compressive strength value, and the fatigue damage percentage. Examining these metrics was intended to provide insight into the efficacy and structural performance of the employed fortification technology. The numerical findings demonstrated that the technique of externally bonding CFRP sheets to strengthen damaged slabs may be regarded as a successful, and cost-effective method.

**Citation:** Hameed, M.O., Daud, R.A. Finite element analysis of fatigue damaged reinforced concrete one-way slabs repaired with CFRP sheets. Magazine of Civil Engineering. 2025. 18(6). Article no. 13805. DOI: 10.34910/MCE.138.5

## 1. Introduction

The majority of the bridges constructed during the past 40 years are made of reinforced concrete. The fatigue damage to the bridges grew as a result of increased traffic volume and load, reducing the spans' service life. Over a bridge's service life, fatigue loading is characterized by a large number of load cycles, which can surpass 100 million. Fatigue loading is induced by moving wheels. Frequent and prolonged load action caused the bridge's rigidity to decrease and demonstrated cumulative deterioration [1]. Concerns regarding the fatigue life and performance of reinforced concrete buildings were growing among academics [2–6]. Because of the increased traffic load and deformed structural parts, there is a noticeable need for improvements to the current transportation infrastructure. Most reinforced concrete slabs and beams will have cracks at some point. Restoring the damaged parts' structural capability requires strengthening and retrofitting [7, 8]. The rehabilitation community has given great attention to the utilization of carbon fiber-reinforced polymer (CFRP) composites among other strengthening solutions because of its durable performance [9]. The inevitable cracking of any structural part is a fact of life. Restoring their flexural capabilities requires strengthening or repairing the injured parts [10–12]. CFRP can be firmly positioned using a bonding agent by inserting it into the tiny groove that has been precut along the cover of a reinforced or prestressed concrete beam or by applying adhesive bonding to the tensile soffit of a structural element.

These CFRP applications are commonly referred to as numerical simulation model (NSM) or employed fortification (EB) strengthening techniques, respectively. Similar to traditional EB CFRP strengthening, NSM CFRP has seen a notable increase in popularity recently in terms of field testing and laboratory study [13]. Improved bond, durability, fatigue performance, quick installation, corrosion resistance, and labor savings are just a few of the numerous noteworthy advantages of NSM CFRP [14–16]. Despite having great tensile strength (more than ten times the yield strength of structural steel, for example) [17], CFRP materials can only be used in a restricted strength range in real-world applications. The rationale is that concrete crushing or CFRP-debonding, as opposed to CFRP-rupture, is often what controls the failure of a CFRP-strengthened concrete part. To get over this constraint and increase the serviceability of a reinforced member even more, NSM CFRP may be post-tensioned. There are several methods for post-tensioning NSM CFRP strips or rods: external jacking apparatus [18, 19], side brackets [20], and embedded anchors [21].

Daud et al. [22] examined how a layer of CFRP adhesive covering one-way reinforced concrete slabs behaved nonlinearly. By forecasting the stiffness deterioration in the concrete for both compression and tension impacts, the finite element (FE) model includes the nonlinearity of the concrete under cyclic loading. A three-dimensional FE model has been presented to more effectively reflect composite sheets' interface and slip profile with the concrete slab under different cyclic loading phases [22]. The authors' experimental data (monotonic and fatigue damage) is used to validate the numerical outputs [23]. This paper's objectives are: (1) to determine interest in expanding our understanding of concrete slab fatigue behavior; (2) to capture the mode of failure and mimic the behavior of damaged one-way slabs, maximum deflection, and ultimate load using an intricate numerical model. (3) A parametric analysis was carried out to determine the impact of adding CFRP thickness, the elastic modulus of CFRP sheet, length of CFRP, and concrete compressive strength and the effect of fatigue-damaged one-way slabs.

## 2. Methods

### 2.1. Numerical Simulation Model

With the help of the universal numerical software suite ABAQUS, the actual model was displayed. Concrete was represented by the isoperimetric eight-node brick element (C3D8R). Every node may move along the *x*, *y*, and *z* axes in three dimensions. The three-dimensional four-node with reduced integration and hourglass control (S4R5) served as a representation of the CFRP sheet. Conversely, the three-dimensional two-node bar element with three-dimensional movements, or truss element (T3D2), represented the reinforced steel rebars. Two-line loads were uniformly applied at the top of each slab in the same location for the experimental test. To represent the end supports of the model properly and in a way that was similar to the tested slabs, displacement boundary conditions were used. Wherever the specimens are supported during experimental testing [23], these boundary requirements must be implemented. Considering that the specimens were only held up by the two shorter edges, as shown in Fig. 1. One supporting line had all of its nodes fixed translated in the *y* and *z* directions, whereas the other supported line had all of its nodes fixed translated in the *x*, *y*, and *z* directions.

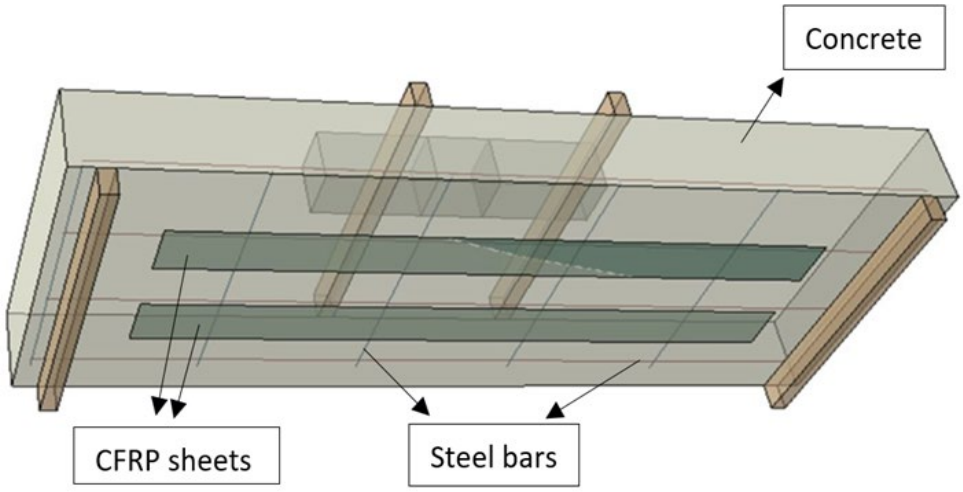


**Figure 1. Boundary condition and applied load isometric view for ends supports.**

## 2.2. Material Models

### 2.2.1. Concrete

Using the yield function from [24], the concrete damaged plasticity model (CDP) was created. This model includes two types of failure processes: tensile cracking and compression fractures. One popular model used to explain concrete's behavior is the CDP. For the nonlinear calculation of concrete members, it is also utilized as it provides an accurate depiction of the material's behavior [25]. The input values for concrete damage plasticity parameters are displayed in Table 1 [26].

***Table 1. Data input for the plasticity parameters of concrete damage [26].***

| | |
|---|---|
| The modulus of Young | 32286.69412 |
| Poisson's ratio | 0.15 |
| Angle of dilation | 36 |
| Eccentricity | 0.1 |
| $\epsilon_{bo}/\epsilon_{co}$ | 1.16 |
| $k_c$ | 0.667 |
| The parameter of viscosity | 0 |

#### 2.2.1.1. Behavior of concrete compressive strength

The compressive strength of concrete is great; the elastic linear route accounts for around 40 % of the overall compressive strength; cracks result in non-linear behavior. According to inelastic concrete stress and strain, respectively, ABAQUS specifies the strain ascending range and descending range. In the present FE study, The Concrete Structure Design Model for Euro Code Two [27] was employed. Table 2 displays data on the compressive strength of concrete [26].

***Table 2. Concrete compressive strength [26]***.

| Yield stress (MPa) | Inelastic strain |
|---|---|
| 7.044263303 | 0 |
| 13.27540985 | 2.88E–05 |
| 18.71156607 | 8.03E–05 |
| 23.37032356 | 0.000156018 |
| 27.26875871 | 0.000255237 |
| 30.42345141 | 0.000377493 |
| 32.85050297 | 0.000522285 |
| 34.56555325 | 0.000689129 |
| 35.58379709 | 0.000877555 |
| 35.92 | 0.001087106 |
| 35.7849029 | 0.001231536 |
| 35.38202351 | 0.001384259 |
| 34.71493152 | 0.001545166 |
| 33.7871334 | 0.001714148 |
| 32.6020739 | 0.001891098 |
| 31.16313731 | 0.00207591 |
| 29.47364884 | 0.002268484 |

#### 2.2.1.2. Concrete tensile behavior

Three parameters may be used in ABAQUS/standard to define the post-cracking tension softening curve: fracture energy, displacement, and strain. The concrete's tensile stress-strain curve utilized in this study was provided by [28] in ABAQUS and had a linear rising line whose gradient matched the concrete's elastic modulus, as well as an exponential slide. Table 3 presents specific facts regarding stress [26].

***Table 3. Specific tension measurements [26]***.

| Yield stress (MPa) | Strain |
|---|---|
| 3.6 | 0 |
| 0.386731643 | 0.031101255 |

### 2.2.2. Steel reinforcement

A bilinear elastic-plastic curve was used in ABAQUS to model the behavior of the steel reinforcement. The plastic curve was constructed using experimental data derived from the stress-strain curve, and the elastic modulus and Poisson's ratio were used to evaluate the behavior's linear elastic zone. Table 4 displays the attributes of steel reinforcement [26].

***Table 4. Steel reinforcement's characteristics [23].***

| | |
|---|---|
| $fy$ | 619 (MPa) |
| $fu$ | 732 (MPa) |
| Poisson's ratio | 0.3 |
| $Es$ | 200 (GPa) |
| elongation | 15% |

### 2.2.3. Carbon fiber reinforced polymer

An orthotropic material was used to mimic the CFRP composite sheet. The behavior is linear until the point of failure. According to the manufacturer's data, the longitudinal elastic main modulus was calculated, and the other two transverse elastic moduli were taken to be around 10 % of the longitudinal elastic main modulus. Additional attributes were presumed based on those delineated by [29]. The elastic characteristics of CFRP sheets are shown in Table 5 [26, 30]. There are other types of carbon fiber, such as plate [31].

***Table 5. Characteristics of CFRP sheet [26].***

| Material | Description | CFRP sheet |
|---|---|---|
| CFRP sheet | Longitudinal modulus (E1), GPa | 230 |
| | Transverse in-plane modulus(E2), GPa | 23 |
| | Transverse out-plane modulus(E3), GPa | 23 |
| | In-plane shear modulus (G12), GPa | 6.894 |
| | Out-of-plane shear modulus (G23), GPa | 4.136 |
| | Out-of-plane shear modulus(G13), GPa | 6.894 |
| | Major in-plane Poisson's ratio, v12 | 0.3 |
| | Out-of-plane Poisson's ratio, v23 | 0.25 |
| | Out-of-plane Poisson's ratio, v13 | 0.25 |

## 2.3. Predefined Field

The fatigue damage stage of damaged slabs may be defined using the ABAQUS/Standard technique. The initial state field presents this strategy. When importing ABAQUS/CAE model data for analysis, at specific points and increments of the research, it is possible to identify the task name linked to the analysis, for which the initial state variable is imported. Any component instance in an ABAQUS/CAE model can be linked to data imported from an earlier ABAQUS/Standard model result. More crucially, before evaluating the data in ABAQUS/Standard, to establish more model definitions, the outcomes and model data could be transferred to new research. This feature permits the application of 50 and 70 % of the ultimate load on specimens with CFRP sheets in this investigation and allows the material condition's distorted model to be utilized as the starting state.

## 2.4. Finite Element Simulation Model Validation

Comparisons with the experimental results are shown in this section. Among these are the load-deflection relationship in the end stage, when monotonic loads and fatigue damage are applied, and the connection between load and deflection when a pressure load is applied following slab repairs. Fig. 2 [23] shows the experimental and numerical results for the monotonic load test in terms of load against deflection relation after the damaged slabs have been fixed. It can be demonstrated that numerical models were, on average, stiffer than experimental data for both the linear and non-linear behavior domains.

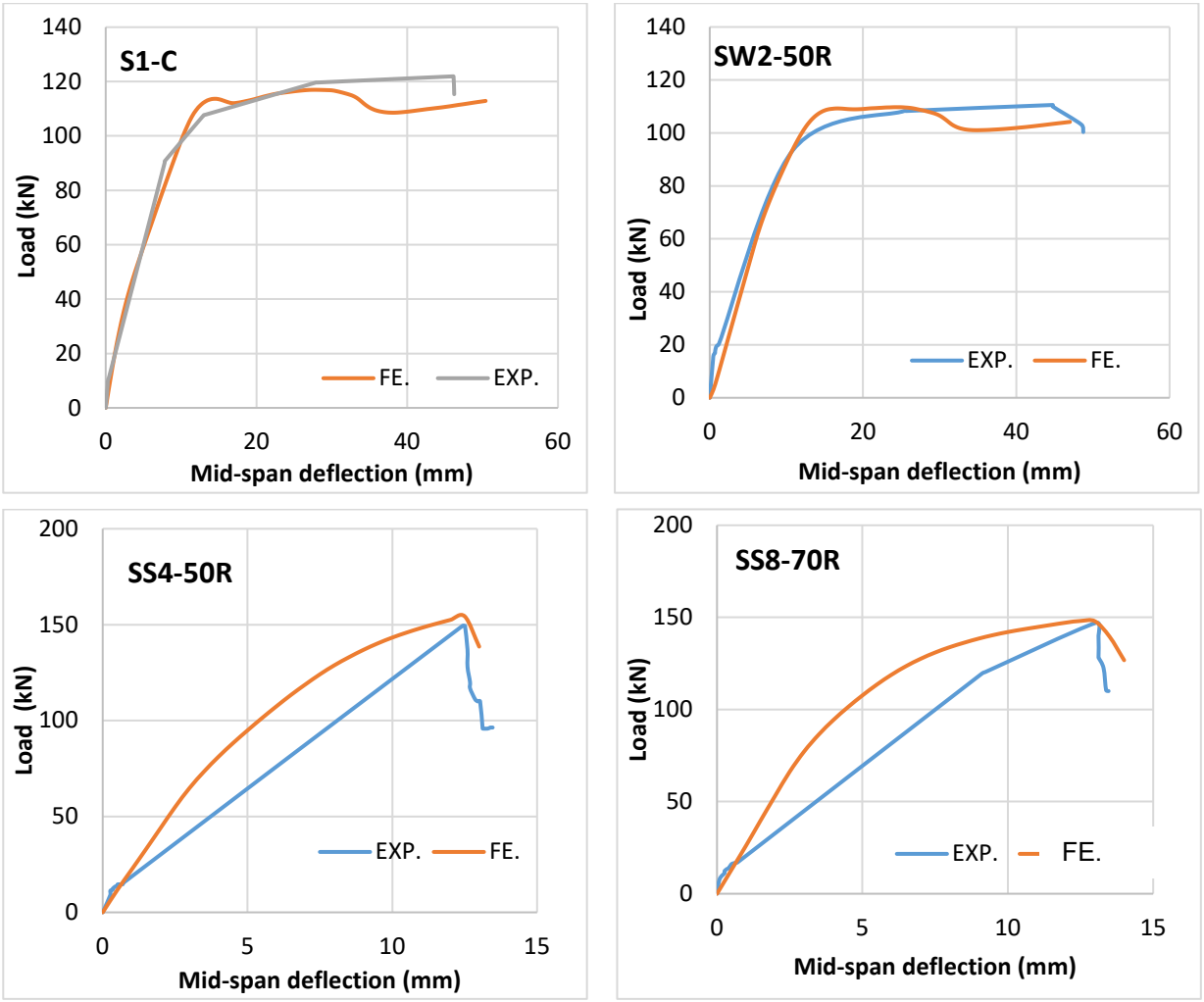


**Figure 2. Numerical and experimental load-deflection curves for selected four slabs [23].**

Table 6 [23] presents a comparison between the failure load and center deflection generated by the FE model and the experimental test conducted at the failure stage (near the failure load) for four slabs under a monotonic test (after fatigue damage). A fair amount of agreement was reached between the deflections and ultimate loads of the FE numerical models, and that was discovered experimentally. For the ultimate loads, the values of the mean and C.V for $(Pu)_{FE}/(Pu)_{Exp}$ were 0.997 and 5.35 %, respectively, and for the deflection of $\delta_{FE}/\delta_{Exp}$, they were 1.197 and 15.99 %, and for energy absorption, they were 1.134 and 12.2 %, respectively.

***Table 6. Failure load and mid-span deflection at failure load, both numerical and experimental [23].***

| Slab's labeling | Failure Load (kN) | | $(Pu)_{FE}/(Pu)_{Exp}$ | Mid-span deflection (mm) | | $\delta_{FE}/\delta_{Exp}$ | Energy Absorption (EA) | | $EA_{FE}/EA_{Exp}$ |
|---|---|---|---|---|---|---|---|---|---|
| | $(Pu)_{Exp}$ | $(Pu)_{FE}$ | | $\delta_{Exp}$ | $\delta_{FE}$ | | $EA_{Exp}$ | $EA_{FE}$ | |
| S1-C | 122 | 117 | 0.959 | 46 | 60 | 1.304 | 4797.8 | 5105.3 | 1.064 |
| SW2-50R | 110.5 | 109.7 | 0.992 | 45 | 47 | 1.044 | 4575.9 | 4353.8 | 0.951 |
| SS4-50R | 149.3 | 154.35 | 1.033 | 12.51 | 15.5 | 1.239 | 1089.6 | 1318.2 | 1.209 |
| SS8-70R | 147 | 148 | 1.006 | 13.03 | 15.7 | 1.204 | 1159.1 | 1525.3 | 1.315 |
| – | Mean | | 0.997 | Mean | | 1.197 | Mean | | 1.134 |
| – | C.V | | 5.35% | C.V | | 15.99% | C.V | | 12.2% |

The load-deflection relationship under applied load, as determined by FE analysis, indicates that the models have more stiffness than the test specimens. There are various possible explanations for the higher stiffness shown in the findings of the FE investigation. The experiment shows how the drying process left the concrete with microcracks, shrinking, and curing. As a result, the specimen's true stiffness would

decrease. The FE models do not consider these microcracks. The FE study deems the link between the steel reinforcement and the concrete to be flawless. This assumption will not hold for the actual specimen. The composite work that exists between the concrete and the steel reinforcement is lost as a result of a bond sliding. The specimen's overall stiffness may thus be lower than that of the FE study.

## 3. Results and Discussion

Using the FE model, based on the experimental data used in this investigation's earlier FE verification. A thorough parametric analysis was carried out. The effects of CFRP sheet thickness are one of the study's variables, CFRP sheet modulus of elasticity, CFRP sheet length, and the concrete compressive strength value.

### 3.1. Effect of Added CFRP Thickness on the Structural Performance of One-Way Slabs

Examined were the effects of the additional CFRP's thickness on the slabs' load-deflection relationship and ultimate load capacity. Based on the CFRP strip's 1000 mm length, three thickness values (one layer, two layers, and four layers) were selected for each thickness with three slabs. Fig. 3 shows the effect of increasing CFRP thickness on the load-mid span deflection relation of slabs. Thicker CFRP sheets increased the rigidity of the slabs, hence raising the maximum load capacity.

According to Table 7, for slab S50-0.34 and S50-0.68, in relation to slab S50-0.17 for group of CFRP fatigue damage equal to 50 %, the percentage of a rise in load capacity is 9.09 and 18.18 %, respectively, and for slab S70-0.34 and S70-0.68, in relation to slab S70-0.17 for group of CFRP fatigue damage equal to 70 %, the percentage of a rise in load capacity is 12.16 and 22.97 %, respectively. The impact of increased CFRP thickness and fatigue damage (50 and 70 %) on ultimate load capacity is depicted in Fig. 4. The debonding CFRP sheet and the concrete surface for each slab were the cause of the failure.

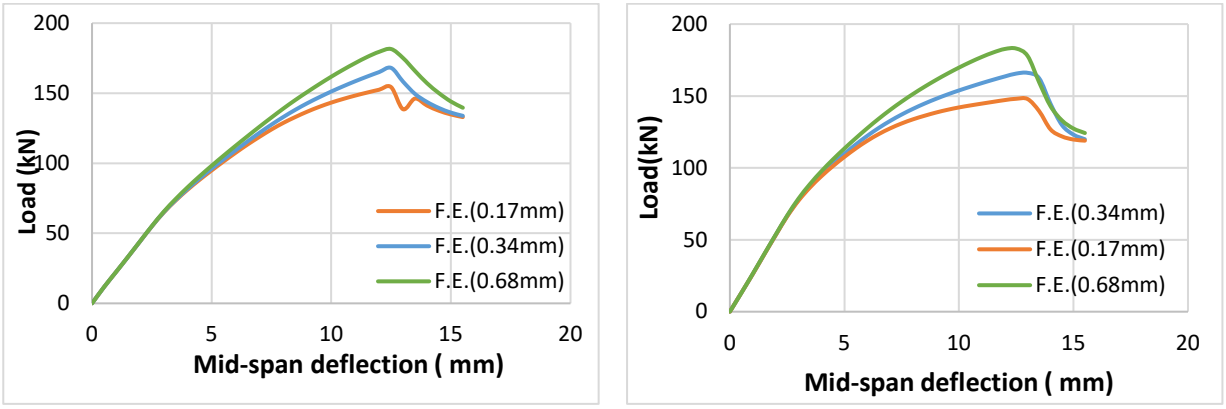


**Fatigue damage 50%** **Fatigue damage 70%**

**Figure 3. Impact of thickness of CFRP sheet on load-mid span deflection curve of slabs.**

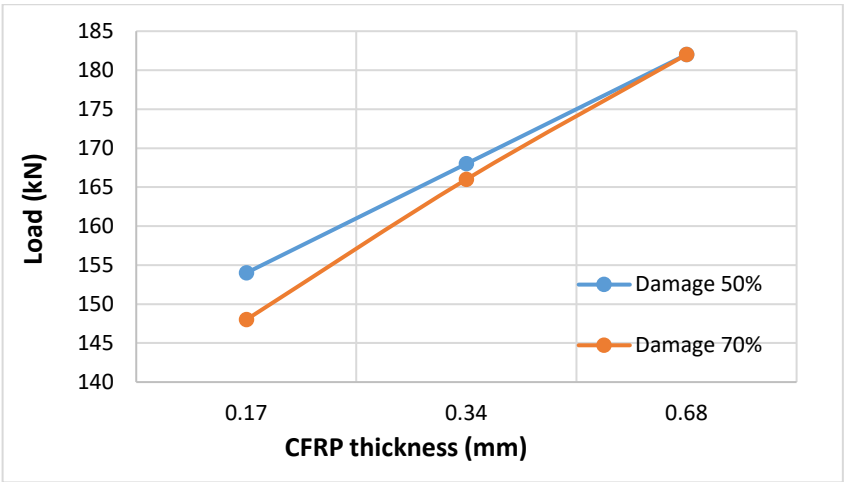


**Figure 4. Impact of CFRP thickness and fatigue damage (50 and 70%) on load capacity.**

***Table 7. The effect of increased CFRP thickness on the load capacity.***

| Slab ID | Length of CFRP sheet (mm) | Thickness of CFRP sheets (mm) | $Pu=P_{ult.}$ (kN) | Increase in $Pu$ percentage relative to $Pu$ of 0.17 mm in each group (%) | Failure mode |
|---|---|---|---|---|---|
| S50-0.17 | 1000 | 0.17 | 154 | Ref. | de-bonding |
| S50-0.34 | 1000 | 0.34 | 168 | 9.09 | de-bonding |
| S50-0.68 | 1000 | 0.68 | 182 | 18.18 | de-bonding |
| S70-0.17 | 1000 | 0.17 | 148 | Ref. | de-bonding |
| S70-0.34 | 1000 | 0.34 | 166 | 12.16 | de-bonding |
| S70-0.68 | 1000 | 0.68 | 182 | 22.97 | de-bonding |

## *3.2. Effect of Added CFRP Modulus of Elasticity on Structural Performance of One-Way Slabs*

For slabs, the impact of the increased CFRP's modulus of elasticity on the load-deflection relationship and ultimate load capacity was investigated. Three values for the modulus of elasticity 160, 230, and 640 GPa were selected. The effect of the additional CFRP strips' modulus of elasticity and fatigue damage (50 and 70 %) on the load-mid span deflection relation of slabs is depicted in Fig. 5. It is evident that adding more CFRP strips with a higher modulus of elasticity made the slabs stiffer, which raised the ultimate load capacity. The impact of CFRP modulus of elasticity and fatigue damage (50 and 70 %) on ultimate load capacity is depicted in Fig. 6.

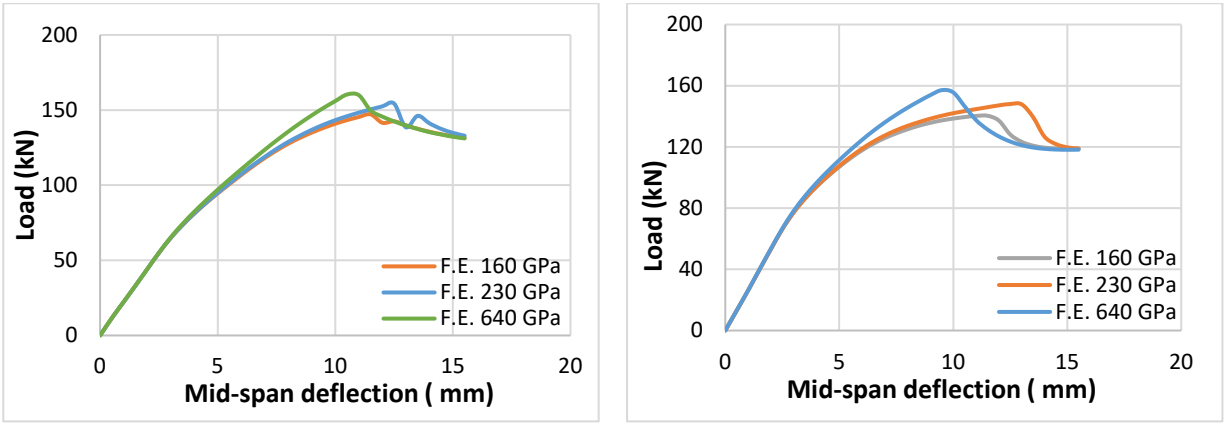


**Figure 5. Impact of modulus of elasticity of CFRP on load of slabs.**

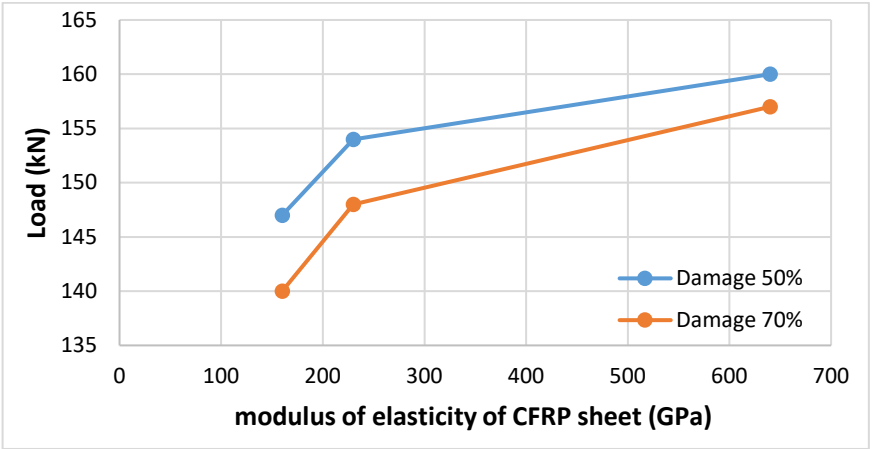


**Figure 6. Impact of modulus of elasticity of CFRP on load relation of slabs.**

According to Table 8, for slab S50-230 and S50-640, compared with slab S50-160 for group of CFRP fatigue damage equal to 50 %, the percentage of an improvement in load capacity is 8.84 and 4.76 %, respectively, while for slab S70-230 and S70-640, compared with slab S70-160 for group of CFRP fatigue damage equal to 70 %, the percentage of the improve in load capacity is 12.14 and 5.71 %, respectively. Debonding the CFRP sheet and the concrete surface for each slab was the cause of the failure.

*Table 8. Impact of modulus of elasticity of CFRP sheet on ultimate load capacity.*

| Slab ID | Length of CFRP sheet (mm) | CFRP sheet modulus of elasticity (GPa) | $Pu=P_{ult.}$ (kN) | Increase in $Pu$ percentage relative to $Pu$ of 160 GPa in each group (%) | Failure mode |
|---|---|---|---|---|---|
| S50-160 | 1000 | 160 | 147 | Ref. | de-bonding |
| S50-230 | 1000 | 230 | 154 | 4.76 | de-bonding |
| S50-640 | 1000 | 640 | 160 | 8.84 | de-bonding |
| S70-160 | 1000 | 160 | 140 | Ref. | de-bonding |
| S70-240 | 1000 | 230 | 148 | 5.71 | de-bonding |
| S70-640 | 1000 | 640 | 157 | 12.14 | de-bonding |

### 3.3. Effect of CFRP Length on One-Way Slabs Structural Performance

Using verified FE modeling (ABAQUS), parametric research was conducted on the application of bonded CFRP sheet in the flexural strengthening of reinforced concrete one-way slabs. This part sought to shed light on the effects of CFRP length by breaking the slab down into two groups: three slabs measuring 600, 800, and 1000 mm each, with 50 % fatigue damage, and three slabs measuring 600, 800, and 1000 mm each, with 70 % fatigue damage. The load-deflection curves of the CFRP length effect are displayed in Fig. 7.

According to Table 9, for slab S50-800 and S50-1000, compared with slab S50-600 for the group of fatigue damage 50 %, the percentage of a rise in ultimate load capacity is 2.19 and 12.4 %, respectively. Similarly, for slab S70-800 and S70-1000, compared with slab S70-600 for the group of fatigue damage 70 %, the percentage of the improve in load capacity is 0.74 and 9.63 %, respectively. Figure 8 illustrates how the ultimate load capacity is affected by the length of CFRP sheets. Debonding between the sheet of CFRP and the surface of concrete for each slab was the cause of the failure.

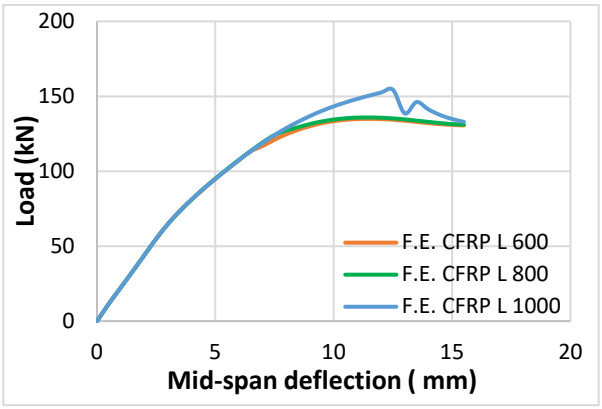


**Fatigue damage 50%**

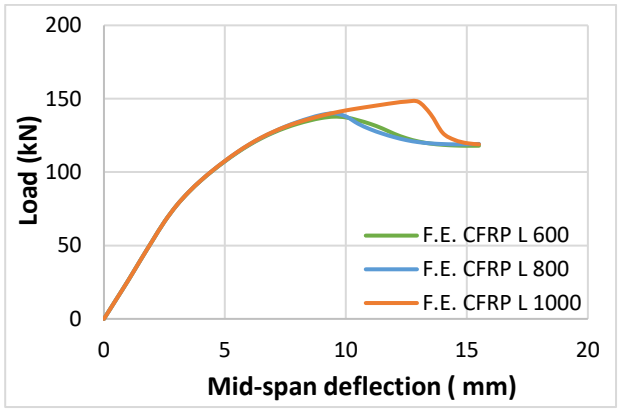


**Fatigue damage 70%**

**Figure 7. Impact of CFRP sheet length on load-mid span deflection relation of slabs.**

*Table 9. Impact CFRP sheet length on ultimate load capacity.*

| Slab ID | No. of CFRP strips *width (mm) | Length of CFRP sheet (mm) | Thickness of CFRP sheets (mm) | $Pu=P_{ult.}$ (kN) | Increase in $Pu$ percentage relative to $Pu$ of length 600mm in each group (%) | Failure mode |
|---|---|---|---|---|---|---|
| S50-600 | 2*100 | 600 | 0.17 | 137 | Ref. | de-bonding |
| S50-800 | 2*100 | 800 | 0.17 | 140 | 2.19 | de-bonding |
| S50-1000 | 2*100 | 1000 | 0.17 | 154 | 12.4 | de-bonding |
| S70-600 | 2*100 | 600 | 0.17 | 135 | Ref. | de-bonding |
| S70-800 | 2*100 | 800 | 0.17 | 136 | 0.74 | de-bonding |
| S70-1000 | 2*100 | 1000 | 0.17 | 148 | 9.63 | de-bonding |

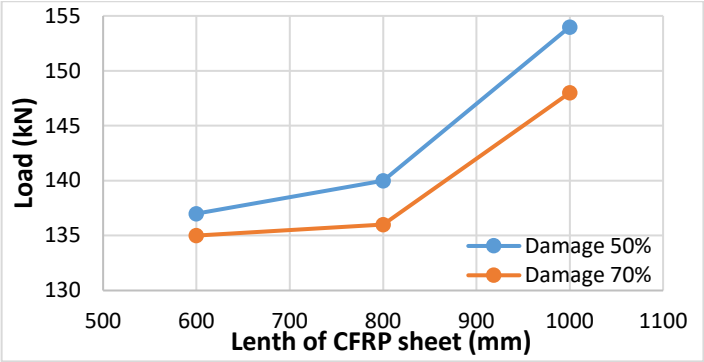


**Figure 8. Effect of length of CFRP sheets on ultimate load.**

### *3.4. Effect of Concrete Compressive Strength Value on Structural Performance of One-Way Slabs*

Three values of the compressive strength of concrete's 25, 35, and 45 MPa, were selected in order to examine the impact of compressive strength of concrete on the ultimate load capacity. The effect of concrete compressive strength on ultimate load capacity is depicted in Fig. 8, and it is evident that as the compressive strength of concrete grows, so will the ultimate load capacity.

According to Table 10, for slab S50-35 and S50-45, in relation to slab S50-25 for the group of CFRP fatigue damage 50 %, the percentage of increased ultimate load capacity is 20.31 and 35.93 %, respectively. Similarly, for the slab S70-35 and S70-45, in relation to the slab S70-25 for the group of CFRP fatigue damage 70 %, the percentage of increased ultimate load capacity is 34.54 and 40.9 %, respectively. Figure 9 illustrates how compressive strength affects ultimate load capacity. The failure was caused by the CFRP sheets and each slab's concrete surface debonding.

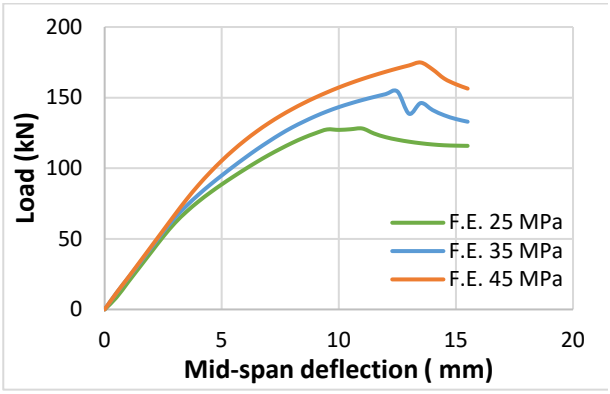


**Fatigue damage 50%**

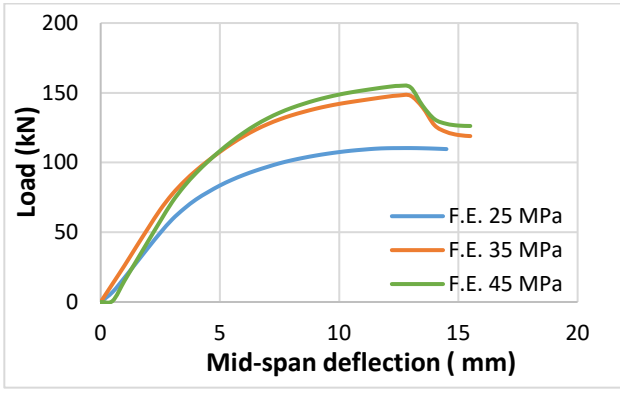


**Fatigue damage 70%**

**Figure 8. Impact of concrete compressive strength on the ultimate load capacity.**

***Table 10. Impact of compressive strength on ultimate load capacity.***

| Slab ID | Compressive strength (MPa) | Length of CFRP sheet (mm) | Thickness of CFRP sheets (mm) | Pu=$P_{ult.}$ (kN) | Increase in Pu percentage relative to Pu of length 600mm in each group (%) | Failure mode |
|---|---|---|---|---|---|---|
| S50-25 | 25 | 1000 | 0.17 | 128 | Ref. | de-bonding |
| S50-35 | 35 | 1000 | 0.17 | 154 | 20.31 | de-bonding |
| S50-45 | 45 | 1000 | 0.17 | 174 | 35.93 | de-bonding |
| S70-25 | 25 | 1000 | 0.17 | 110 | Ref. | de-bonding |
| S70-35 | 35 | 1000 | 0.17 | 148 | 34.54 | de-bonding |
| S70-45 | 45 | 1000 | 0.17 | 155 | 40.9 | de-bonding |

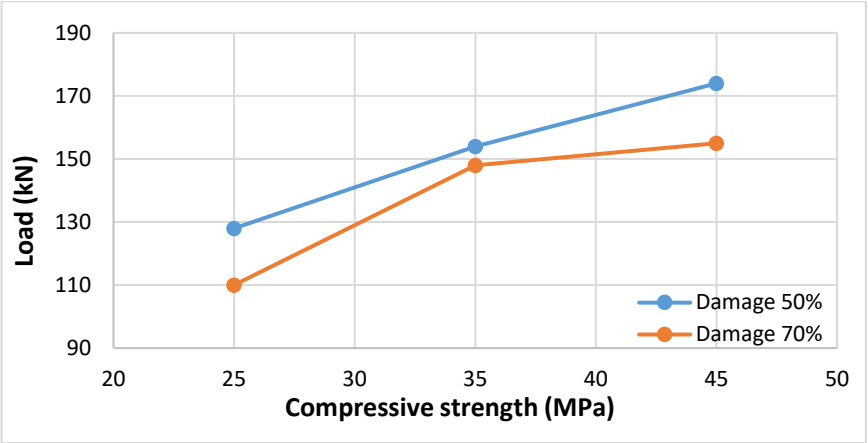


**Figure 9. Impact of compressive strength on load capacity.**

## 4. Conclusions

1. A reasonable degree of agreement was reached between the deflections, ultimate loads, and energy absorption of FE models obtained through numerical methods and those discovered through experimentation. For example, the values of the mean and C.V for ultimate loads for $(Pu)_{FE}/(Pu)_{Exp}$ were 0.997 and 5.35 %, respectively, while for deflection of $\delta_{FE}/\delta_{Exp}$, values of mean and C.V were 1.197 and 15.99 %, respectively, and for energy absorption, the values of the mean and C.V were 1.134 and 12.2 %, respectively.
2. A numerical analysis was conducted to examine the impact of CFRP thickness on ultimate load capacity. For slab S50-0.34 and S50-0.68, in relation to slab S50-0.17 for group of CFRP fatigue damage equal to 50 %, the percentage of the rose in load capacity is 9.09 and 18.18 %, respectively, and for slab S70-0.34 and S70-0.68, in relation to slab S70-0.17 for group of CFRP fatigue damage equal to 70 %, the percentage of the rose in load capacity is 12.16 and 22.97 %, respectively.
3. A numerical analysis was conducted to determine how the CFRP modulus of elasticity affected the ultimate load capacity. For slab S50-230 and S50-640, in relation to slab S50-160 for a group of CFRP fatigue damage equal to 50 %, the percentage of increased ultimate load capacity is 8.84 and 4.76 %, respectively, and for slab S70-230 and S70-640, in relation to slab S70-160 for a group of CFRP fatigue damage equal to 70 %, the percentage of increased ultimate load capacity is 12.14 and 5.71 %, respectively.
4. A numerical analysis was conducted to examine the impact of CFRP sheet length on ultimate load capacity. The results showed that the percentage increases in load capacity for slab S50-800 and S50-1000, in relation to slab S50-600 for the CFRP fatigue damage 50 % group, were 2.19 and 12.4 %, respectively, and for the slab S70-800 and S70-1000, in relation to the slab S70-600 for the CFRP fatigue damage 70 % group, were 0.74 and 9.63 %, respectively.
5. A numerical study was used to examine how the compressive strength of concrete affected the structural performance of slabs. Findings indicated that the ultimate load capacity rose by a percentage for slab S50-35 and S50-45, related to slab S50-25 for the group of CFRP fatigue damage 50 %, was 20.31 and 35.93 %, respectively, while for slab S70-35 and S70-45 related to slab S70-25 for the group of CFRP fatigue damage 70 %, the percentage increase in load capacity was 34.54 and 40.9 %, respectively.

## References

1. Zhang, J., Li, P., Mao, Y., Dong, Zh. The Mechanical Properties of Reinforced Concrete Plate-Girders when Placed Under Repeated Simulated Vehicle Loads. Materials. 2019. 12(11). Article no. 1831. DOI: 10.3390/ma12111831
2. Do, M.-T., Chaallal, O., Aïtcin, P.-C. Fatigue Behavior of High-Performance Concrete. Journal of Materials in Civil Engineering. 1993. 5(1). Pp. 96–111. DOI: 10.1061/(ASCE)0899-1561(1993)5:1(96)
3. Holmen, J.O. Fatigue of Concrete by Constant and Variable Amplitude Loading. ACI Special Publication. 1982. 75. 71–110.
4. Chen Hao-jun, Peng Yi-bin, Zhang Qi-sen. Research on Fatigue Behavior of Concrete Beams Reinforced by Cold-Rolled Deformed Steel Bar. China Journal of Highway and Transport. 2006. 19(1). Pp. 23–27.
5. Schläfli, M., Brühwiler, E. Fatigue of existing reinforced concrete bridge deck slabs. Engineering Structures. 1998. 20(11). Pp. 991–998. DOI: 10.1016/S0141-0296(97)00194-6
6. Wang Chun-sheng, Zhou Jiang, Wu Quan-you, Wang Yu-jiao, Dong Xiao-hong. Fatigue Life and Service Safety Assessment for Existing Concrete Bridges. China Journal of Highway and Transport. 2012. 25(6). Pp. 101–107.

7. Daud, S.A., Daud, R.A., Al-Azzawi, A.A. Behavior of reinforced concrete solid and hollow beams that have additional reinforcement in the constant moment zone. Ain Shams Engineering Journal. 2021. 12(1). Pp. 31–36. DOI: 10.1016/j.asej.2020.07.017
8. Najm, I.N., Daud, R.A., Al-Azzawi, A.A. Behavior of reinforced concrete segmental hollow core slabs under monotonic and repeated loadings. Structural Monitoring and Maintenance. 2019. 6(4). Pp. 269–289. DOI: 10.12989/smm.2019.6.4.269
9. Bakis, Ch.E., Bank, L.C., Brown, V.L., Cosenza, E., Davalos, J.F., Lesko, J.J., Machida, A., Rizkalla, S.H., Triantafillou, Th. Fiber-Reinforced Polymer Composites for Construction – State-of-the-Art Review. 2002. 6(2). Pp. 73–87. DOI: 10.1061/(ASCE)1090-0268(2002)6:2(73)
10. Lateef, H.E., Al-Allaf, M.H., Daud, R.A. Experimental study on bond-slip behavior of NSM-CFRP plate and recycled aggregates concrete substrate. Innovative Infrastructure Solutions. 2024. 9(10). Article no. 368. DOI: 10.1007/s41062-024-01699-9
11. Daud, R.A., Daud, S.A., Al-Azzawi, A.A. Tension stiffening evaluation of steel fibre concrete beams with smooth and deformed reinforcement. Journal of King Saud University – Engineering Sciences. 2021. 33(3). Pp. 147–152.
12. Al-Allaf, M.H., Daud, RA, Daud, SA. Nonlinear Finite Element analysis of concrete corbels with hybrid reinforcements. Mechanics of Advanced Materials and Structures. 2024. 32(21). Pp. 5245–5255. DOI: 10.1080/15376494.2024.2420910
13. Jasim, N.R., Daud, R.A. Behavior of hollow core slabs strengthened by NSM CFRP plates subjected to repeated loading. AIP Conference Proceedings. 2024. 3009(1). Article no. 030086. DOI: 10.1063/5.0193577
14. Fernandes, P.M.G., Silva, P.M., Sena-Cruz, J. Bond and flexural behavior of concrete elements strengthened with NSM CFRP laminate strips under fatigue loading. Engineering Structures. 2015. 84. Pp. 350–361. DOI: 10.1016/j.engstruct.2014.11.039
15. Dalfré, G.M., Barros, J.A.O. NSM technique to increase the load carrying capacity of continuous RC slabs. Engineering Structures. 2013. 56. Pp. 137–153. DOI: 10.1016/j.engstruct.2013.04.021
16. Peng, H., Zhang, J., Cai, C.S., Liu, Y. An experimental study on reinforced concrete beams strengthened with prestressed near surface mounted CFRP strips. Engineering Structures. 2014. 79. Pp. 222–233. DOI: 10.1016/j.engstruct.2014.08.007
17. ACI Committee 440. ACI 440R-07. Report on fiber reinforced polymer (FRP) reinforcement for concrete structures. American Concrete Institute. Farmington Hills, MI, 2007.
18. Wu, Zh., Iwashita, K., Sun, X. Structural Performance of RC Beams Strengthened with Prestressed Near-Surface-Mounted CFRP Tendons. Case Histories and Use of FRP for Prestressing Applications. American Concrete Institute. Farmington Hills, MI, 2007. Pp. 165–178.
19. Choi, H.T., West, J.S., Soudki, Kh.A. Effect of Partial Unbonding on Prestressed Near-Surface-Mounted CFRP-Strengthened Concrete T-Beams. Journal of Composites for Construction. 2011. 15(1). Pp. 93–102. DOI: 10.1061/(Asce)Cc.1943-5614.0000149
20. El-Hacha, R, Gaafar, M. Flexural strengthening of reinforced concrete beams using prestressed, near-surfacemounted CFRP bars. PCI Journal. 2011. 56(4). Pp. 134–151. DOI: 10.15554/pcij.09012011.134.151
21. De Lorenzis, L., Micelli F, La Tegola A. Passive and active near surface mounted FRP rods for flexural strengthening of RC beams. Proceedings of the Third International Conference on Composites in Infrastructure. CD-ROM version. Paper no. 83. San-Francisco, CA, 2002.
22. Daud, R., Cunningham, L., Wang, Y. Non-linear FE Modelling of CFRP-strengthened RC slabs under cyclic loading. Athens Journal of Technology and Engineering. 2015. 2(3). Pp. 161–180.
23. Hameed, M.O., Daud, R.A. Behavior of Fatigue Damaged Reinforced Concrete One-Way Slabs Repaired with CFRP Sheets. Civil And Environmental Engineering. 2024. 20(1). Pp. 364–376. DOI: 10.2478/cee-2024-0028
24. Lubliner, J., Oliver, J., Oller, S., Oñate, E. A plastic-damage model for concrete. International Journal of Solids and Structures. 1989. 25(3). Pp. 299–326. DOI: 10.1016/0020-7683(89)90050-4
25. Tyau, J.S. Finite element modeling of reinforced concrete using 3-dimensional solid elements with discrete rebar. Ph.D. thesis. Brigham Young University, 2009.
26. BS EN 1992-1-1. Eurocode 2: Design of concrete structures: Part 1–1: General rules and rules for buildings. British Standards Institution, 2004.
27. Wang, T., Hsu, Th.T.C. Nonlinear finite element analysis of concrete structures using new constitutive models. Computers & Structures. 2001. 79(32). Pp. 2781–2791. DOI: 10.1016/S0045-7949(01)00157-2
28. Reddy, J.N. Mechanics of Laminated Composite Plates and Shells: Theory and Analysis. CRC Press. Boca Raton, 2003. 858 p. DOI: 10.1201/b12409
29. Hibbitt, K., Karlsson, B.I., Sorenson, E.P. Virtual work. ABAQUS/Standard theory manual. Sorenson Inc, 2016. Pp. 421–422.
30. Abbood K.A., Daud R.A. Preloaded behavior of thick one-way slabs strengthened with NSM–CFRP plates. NeuroQuantology. 2022. 20(6). Pp. 8665–8679. DOI: 10.14704/nq.2022.20.6.NQ22858
31. Abbood K.A., Daud R.A. Experiment Investigation of Behavior of Preloaded Thick One-Way Slabs Repaired by NSM CFRP Plate. Mathematical Statistician and Engineering Applications. 2022. 71(4). Pp. 3695–3708. DOI: 10.17762/msea.v71i4.931


***Information about the authors:***


***Mohammed Hameed***,
*E-mail: st.mohammed.a.h.f@nahrainuniv.edu.iq*

***Raid Daud***,
*E-mail: raid.a.daud@nahrainuniv.edu.iq*


*Received 08.06.2024. Approved after reviewing 23.12.2024. Accepted 14.01.2025.*